

## MODELLING OF PRE-STRESSED CONCRETE BEHAVIOUR IN THE TEMPERATURE RANGE 20-40°C

A. SELLIER<sup>\*\*†</sup>, T. VIDAL<sup>\*\*††</sup>, F. MANZONI<sup>\*\*†††</sup>, L. LACARRIERE<sup>\*\*††††</sup>, H. CAGNON<sup>\*\*†††††</sup>

\*LMDC, Université de Toulouse, INSA/UPS Génie Civil, 135 Avenue de Ranguel, 31077 Toulouse cedex 04, France.

† e-mail: [alain.sellier@univ-tlse3.fr](mailto:alain.sellier@univ-tlse3.fr)

†† e-mail: [thierry.vidal@univ-tlse3.fr](mailto:thierry.vidal@univ-tlse3.fr)

††† e-mail: [manzoni@insa-toulouse.fr](mailto:manzoni@insa-toulouse.fr)

†††† e-mail: [laurie.lacARRIERE@insa-toulouse.fr](mailto:laurie.lacARRIERE@insa-toulouse.fr)

††††† e-mail: [cagnon@insa-toulouse.fr](mailto:cagnon@insa-toulouse.fr)

**Key words:** Creep, pre-stressing, transient thermal creep, finite elements

**Abstract:** Assessing behaviour of pre-stressed concrete structures in a context of temperature variation is a major of concern when dealing with a scenario of accident in a nuclear power plant, or of storage of exothermic nuclear wastes in underground concrete tunnels. In order to improve the reliability of finite element models usable for such applications, several experimental programs [1,2] and a numerical model [3,4] were carried out in LMDC Toulouse. Among the experiments, some concrete cylinders and pre-stressed concrete beams submitted to creep at 20°C and 40°C were studied [2] and the provided results used to calibrate or improve the model. The numerical model combines non-linear visco-elasticity, plasticity and anisotropic damage in a poro-mechanics context. The model is able to consider benefits and deleterious effects of capillary pressures associated with temperature and water saturation variations. The paper focuses on the numerical implementation of the non-linear visco-elastic behaviour of concrete [4] and of pre-stressed wires [5], and on the model's applications to concrete specimens studied in the temperature range from 20°C to 40°C.

## 1 INTRODUCTION

The paper starts with the principles of the experimental program designed in the framework of the French research national project MACENA to provide data for model fitting and validations. Fitting are done at the material scale on concrete cylinders, while validations are based on results of pre-stressed concrete beams subjected later to bending loads and temperature rises . The second part of the paper summarizes the main originalities of the model clarified to consider concrete's evolutions in variable thermo-mechanical conditions. The method proposed to simplify the mesh of large concrete structures, the principle of damage criteria able to consider effects of moisture and temperature, and the principles of creep modeling are also exposed. After a brief recall of the pre-stressing wire relaxation model, the paper gives an example of model's data fitting on concrete cylinders at 20°C and 40°C for two loading levels. The last section concerns the application of the model to the pre-stressed concrete beams. This section shows that, after a minimalist adjustment of one parameter to consider a lack of knowledge of concrete aging until the date of pre-stressing, the model is able to simulate the beam's behaviours. After this stage of validation, internal variables of the model allow the users to easily access to concrete damage, stresses in concrete, wire, and reinforcements. Even if the model needs yet some validations in other thermo-hydric conditions, its applicability to large structures such as nuclear power plant vessels is a realistic perspective.

## 2 EXPERIMENTAL PROGRAM

### 2.1 Material and experimental setups

The concrete characteristics are given in table 1. This concrete was tested in two geometric configurations. First, behaviour and creep laws are identified on cylindrical

specimens 11 cm diameter and 22 cm height. Secondly, pre-stressed beams schemed in figure 1 are axially pre-stressed at 12 MPa, corresponding to around 30% of concrete compressive strength, by means of steel wires, and then placed in flexural condition to provoke a flexural state doubling the theoretical compressive stress on one fiber of the mid span cross-section (24MPa) and canceling it on the other one (0MPa).

**Table 1** : Concrete characteristics

Concrete Characteristics	
Compressive strength Rc (MPa)	46.1
Tensile strength Rt (MPa) <sup>(1)</sup>	3.9
Fracture Energy Gf (J/m <sup>2</sup> )	100.0
Young's modulus E (GPa)	35.1
Coefficient of thermal expansion $\alpha$	12e-6

(1) at 20°C, 92% water saturation

For concrete cylinders, the loading chronology consists of a first stage during which the concrete specimens are stored in autogenous conditions, followed by a mechanical loading at 30% Rc or 60% Rc. One day after mechanical loading, the temperatures are either kept constant at 20°C or increased until 40°C. The temperature rising was 0.1°C/ mn. For beams, the axial pre-stress of 12 MPa is applied thanks to the steel wire. Between the pre-stressing day and the start of bending, the concrete creeps and the wire relaxes, leading to a classical loss of pre-stressing. The beams at 20°C are loaded in flexion 250 days after the pre-stressing, the ones at 40°C are loaded 125 days after pre-stressing.

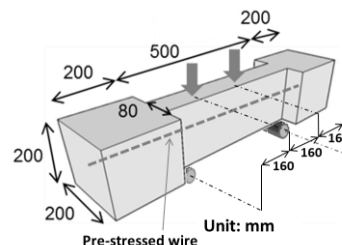


**Figure 1**: Pre-stressed beam and loading setup.

The pre-stressing wires are non-adherent to the concrete, and passive reinforcements are added to limit the risk of brittle fracture of the beams. The wire characteristics are given in table 2.

**Table 2 :** Pre-stressing wires characteristics

Pre-stressing wires (T15S)	
Characteristic tensile strength $f_{pk}$ (MPa)	1860
Characteristic 0.1 % proof-stress of prestressing steel $f_{p0.1k}$ (MPa)	1650
Diameter (mm)	1.57
Cross section (mm <sup>2</sup> )	150

The passive and transverse reinforcements scheme is given in figure 2. The beams and the concrete characteristics are more detailed in [2]. Concerning the pre-stressing wire, a complete identification of their behaviour is already published in [5,6].

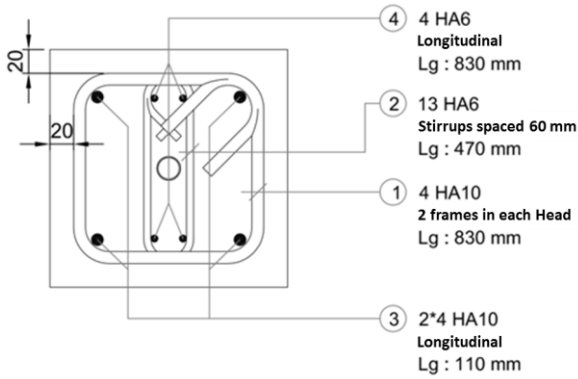


**Figure 2:** Cross section with passive and transverse reinforcements, and central location of the wire.

### 3 MODEL PRINCIPLE

The model was clarified to be used in large reinforced concrete structures, which involved two constraints: first, the wires and reinforcements have not to be explicitly meshed to avoid two heavy meshes when modeling the whole nuclear vessel [7], and secondly all the major components of wires, reinforcements and concrete behaviours have to be considered. These components can be classified in three categories: visco-elastic (for creep of concrete and relaxation of wires), plastic (for permanent strains in each

material), and damage, mainly to consider the cracking of concrete. The components are combined as schemed in figure 3.

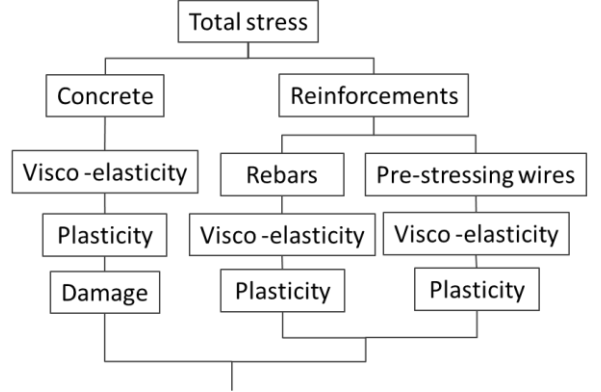


**Figure 3:** Components of the homogenized behaviour law for reinforced concrete.

#### 3.1 Homogenized behaviour law

The homogenized reinforced concrete behaviour law is obtained by combination of concrete and reinforcements (1).

$$\sigma = \left(1 - \sum_{r=1}^n \rho_r\right) \sigma^c + \sum_{r=1}^n \rho_r \sigma_r \vec{e}_r \otimes \vec{e}_r \quad (1)$$

In equation (1)  $\sigma^c$  is the stress tensor in the concrete,  $\rho_r$  reinforcement's densities,  $\sigma_r$  the stress in the reinforcement number  $r$  oriented in the direction  $\vec{e}_r$ . Each reinforcement can be either a pre-stressing wire or a passive rebar. This method allows also to consider the sliding between reinforcements and concrete without meshing the reinforcements. the principle consists of using a Helmholtz formulation which links the RC strain  $\varepsilon$  to the reinforcement strain (equation 2). Details concerning this aspect are published in [7].

$$\varepsilon^{re} - \frac{E^r D^r}{4H^i} \frac{\partial^2 \varepsilon^{re}}{\partial x^2} = \bar{\varepsilon} - \varepsilon^{rp} - \varepsilon^{rv} \quad (2)$$

In this equation,  $E^r$  is the Young's modulus of the reinforcement,  $H^i$  the secant modulus of the interface behavior law [7],  $D^r$  the diameter of the rebar,  $\varepsilon^{re}$  its elastic strain,  $\varepsilon^{rp}$  its plastic

strain,  $\varepsilon^{TV}$  its viscous strain (causing relaxation), and  $\bar{\varepsilon}$  the mechanical strain of the reinforced concrete. Thanks to this equation, the sliding of pre-stressed wire and passive reinforcements can be treated numerically without meshing them as illustrated in figure 8.

### 3.2 Concrete behavior law

As specified in equation (3), the concrete behaviour law considers elastic strain  $\varepsilon^e$ , thermal dilations  $\varepsilon^T$ , creep strains  $\varepsilon^c$ , transient thermal deformation  $\varepsilon^f$ , permanent strains corresponding to localized cracks opening  $\varepsilon^{pt}$ , and permanent strains corresponding to diffuse shear cracking  $\varepsilon^{ps}$ .

$$\varepsilon^e = \varepsilon - \varepsilon^T - \varepsilon^c - \varepsilon^f - \varepsilon^{pt} - \varepsilon^{ps} \quad (3)$$

The stiffness tensor  $\mathbf{C}^0$  of the sound material allows computing the effective stress with equation (4).

$$\tilde{\sigma}^c = \mathbf{C}^0 \varepsilon^e \quad (4)$$

In equation (4),  $\tilde{\sigma}^c$  is the effective stress (in the sense of damage). The apparent stress is deduced from this last using equation (5).

$$\sigma^c = (1 - D^s)(\tilde{\sigma}^{ct}(\mathbf{1} - \mathbf{D}^t) + \mathbf{R}^c \tilde{\sigma}^{cc}) \quad (5)$$

In (5) a spectral decomposition of the effective stress tensor  $\tilde{\sigma}^c$  in positive part  $\tilde{\sigma}^{ct}$  and negative part  $\tilde{\sigma}^{cc}$  is done to consider the effects of tensile damage tensor  $\mathbf{D}^t$ , crack re-closing function  $\mathbf{R}^c$  and isotropic shear damage  $D^s$ . The evolution laws of the main values of the damage tensors depend on permanent strains  $\varepsilon^{pt}$  and  $\varepsilon^{ps}$  respectively for  $\mathbf{D}^t$  and  $D^s$ . These strains are computed to verify orthotropic Rankine criteria (also known as principal stresses criteria) in tension and a Drucker Prager criterion for shear. Details of these criteria can be found in [3] and [7], and an example of the behaviour law is given in figure 4. The details of tensile loading cycles at different saturation degrees and

temperatures, given in figure 5, show that the capillary forces are considered in the behaviour law. To obtain this effect, the assumption of a competition between cohesion and cracking effects of capillary forces, at the micro-scale, are considered in the orthotropic Rankine criteria  $f_I^R$  (equation 6). In these criteria, the water pressure  $P^w$  depends on the saturation  $S_r$  and the temperature  $T$ , through the water sorption curve as explained in [8]. This pressure multiplied by the stress concentration coefficient  $K^w$  acts in addition to the applied effective stress  $\tilde{\sigma}_I$  in the loading part of the criteria, and in the strength part through the classical Biot coefficient  $b$  in complement of the tensile strength in saturated condition  $\tilde{R}_{sat}^t$ .

$$f_I^R = (\tilde{\sigma}_I - K^w b S_r P^w) - (\tilde{R}_{sat}^t - b S_r P^w) \quad (6)$$

The poro-mechanics criteria (6) are then used to compute the plastic strains  $\varepsilon^{pt}$  and the tensile damages  $\mathbf{D}^t$  used in equation (5). Note a negative loading  $\tilde{\sigma}_I$  can prevent the plastic strains and the damages associated to these criteria.

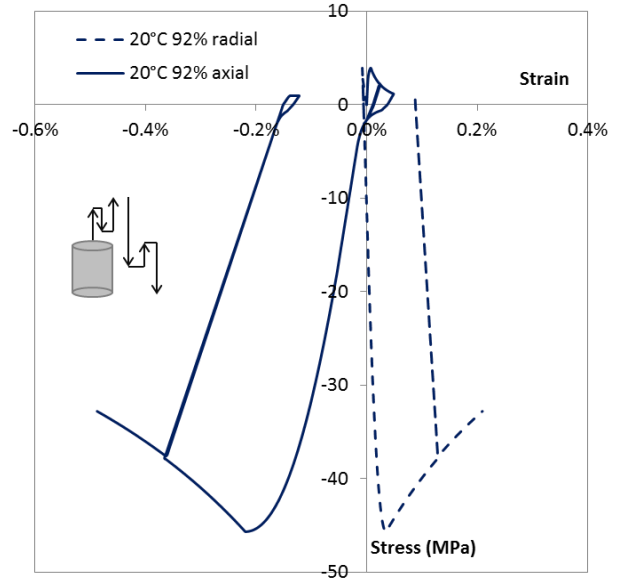


**Figure 4:** Modelling of a uniaxial cyclic test for the concrete alone.

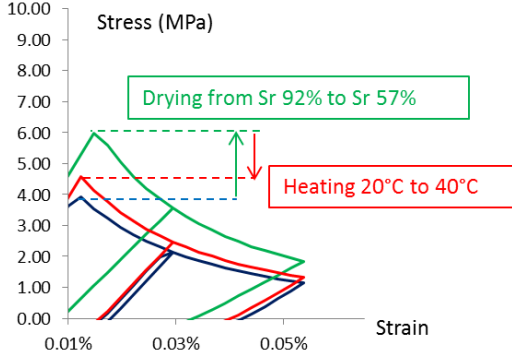


**Figure 5:** Modelling of the effects of capillary forces on the tensile behaviour law of concrete (fitted with results from the research project MOSAIC [9] for the effects of drying, and from MACENA for the temperature effect).

According to [10], the creep strain  $\varepsilon^c$  is the main cause of pre-stresses loss in nuclear containment vessel. In the model used in the present work [4], the creep velocity is assumed proportional to the loading through the elastic strain  $\varepsilon^e$  (equation 7). In (7),  $\tau$  is a characteristic time tensor which controls the creep rate of concrete. To consider the reduction of creep strain with time, the characteristic time evolve according to equation (8).

$$\frac{\partial \varepsilon^c}{\partial t} = \frac{\varepsilon^e}{\tau^c} \quad (7)$$

In equation (8),  $\tau^{ref}$  is a reference value of the characteristic time for un-consolidated concrete (never loaded), and  $C_v^T$  takes into account the modification of concrete viscosity in temperature thanks to an Arrhenius law with an activation energy of 17 kJ/mol [11];  $C_v^H$  considers the effect of drying on creep velocity, it is the inverse of the water saturation rate  $S_r$ , and  $C_I^c$  is the consolidation function considering the stress redistribution between viscous and non-viscous phases during the creep process in each principal direction number  $I \in [1,2,3]$ . So, the consolidation is an anisotropic phenomenon (see [4] for the justification of this theory).

$$\tau_I = \tau^{ref} C_v^T C_v^H C_I^c \quad (8)$$

In a given direction  $I$ , the evolution of the consolidation function, which is the main originality of the creep model [4], is given by equation (9), in which  $k$  controls the creep “potential”.

$$C_I^c = \frac{1}{k} \exp\left(\frac{\varepsilon_I^c}{k \varepsilon_I^e}\right) \quad (9)$$

The coefficient  $k$  depends on the environmental and loading conditions (equation 10). Coefficient  $C_p^T$  considers the effects of temperature on creep potential. According to Ladaoui et al. [11,12], these effects are measurable above 45°C.  $C_p^M$  allows to provoke tertiary creep if the material is too much loaded (this aspect, already published in [4], is not detailed in the present work).

$$k = C_p^T C_p^M \frac{E \varepsilon_k^m}{\sigma_k} \quad (10)$$

In (10),  $\varepsilon_k^m$  is a parameter obtained by fitting, it controls the consolidation phenomenon.

In equation (3), another viscous strain called  $\varepsilon^f$  exists. This is a short term strain observed only when a concrete already loaded during a short period is heated rapidly. In the bibliography, this strain is often qualified of “Transient Thermal Deformation i.e TTD”. In the present work, this strain is modeled using a double scale porosity model explained in the details in [13]. The principle consists of provoking a viscous strain (equation 11), while the water located into the C-S-H bundles is subjected to a pressure  $P^{CSH}$  greater than the capillary pressure  $P^w$ . This phenomenon could be due to the restrained dilation of water contained in C-S-H bundles during rapid heating of concrete. It disappears rapidly due to the diffusion of the over amount of water from the C-S-H to the capillary pores. The duration of the TTD and its amplitude are

controlled, in the model, by the pressure  $P^{CSH}$  according to equations (11, 12, 13).

$$\frac{\partial \boldsymbol{\varepsilon}^f}{\partial t} = \frac{\boldsymbol{\varepsilon}^e}{\boldsymbol{\tau}^f} \quad (11)$$

In (11), the characteristic time  $\boldsymbol{\tau}^f$  is assessed using equation (12), and, in (13),  $\Delta P_{ref}^{CSH}$  is a fitting parameter given in table 4.

$$\boldsymbol{\tau}^f = \tau^{ref} C_v^T C_v^{CSH} C_I^c \quad (12)$$

In equation (12), the thermal effect on creep potential and  $C_v^T$  and the consolidation coefficient  $C_I^c$  are the same than in equation (8), only  $C_v^{CSH}$  replaces  $C_v^H$  to consider the amplification effect of the C-S-H inner pressure  $P^{CSH}$  (13).

$$C_v^{CSH} = \frac{\Delta P_{ref}^{CSH}}{[P^{CSH} - P^w]^+} \quad (13)$$

The decrease of the water pressure in C-S-H is computed using the diffusion equation (14) which controls the micro-diffusion of water from C-S-H porosity to the capillary porosity.

$$\frac{\partial P^{CSH}}{\partial t} = \frac{[P^{CSH} - P^w]}{\tau_{ref}^{CSH} C_v^H} \quad (14)$$

In (14),  $\tau_{ref}^{CSH}$  is a parameter fitted to obtain a realistic duration of the TTD. In the simulation presented in figure 6, the phenomenon of TTD occurs, it is the cause of the rapid creep at 40°C during heating, because in these tests, the loading occurs just one day before heating, and the heating rate is relatively fast (0.1°C / mn).

### 3.3 Pre-stressed wires behaviour law

The pre-stressed wires are modeled using a uniaxial behaviour law considering both the

plastic  $\varepsilon_r^p$  and viscous strains  $\varepsilon_r^v$  (equation 15).

$$\sigma_r = E_r(\bar{\varepsilon}_r - \varepsilon_r^p - \varepsilon_r^v) \quad (15)$$

In (15),  $E_r$  is the Young's modulus of the steel wire,  $\bar{\varepsilon}_r$  its total mechanical strain. The plastic strain  $\varepsilon_r^p$  is controlled thanks to a kinematic plasticity model with a linear hardening. The originalities of the reinforcements modeling are that, first, the  $\bar{\varepsilon}_r$  is not equal to the concrete one because the sliding between concrete and steel is considered thanks to equation (2), and, secondly, the relaxation of the wires is considered through the viscous strain  $\varepsilon_r^v$ . This last is computed thanks to a non-linear viscous law quite similar to the one used for concrete but with appropriated parameters.

$$\frac{\partial \varepsilon_r^v}{\partial t} = \frac{\varepsilon_r^e}{\tau^r} \quad (16)$$

In (16)  $\varepsilon_r^e$  is the elastic strain of the wire and  $\tau^r$  a characteristic time controlled by a consolidation equation, in the same way than in equation (9), but with parameters fitted on relaxation tests described in [5].

## 4 MODEL FITTING

### 4.1 Fitting of the creep law for the concrete

The fitting procedure consists of adopting the parameters given in table 1 and of adjusting the creep model parameters in order to reproduce the behaviour of cylinder specimens heated and loaded in different conditions. In figure 6, the theoretical curves are compared to the experimental ones. The fitted parameters are given in table 3. It is worth noting that the model parameters are fitted in cases 20°C 30% and 60%Rc, and 40°C 30%Rc. The simulation of the case 40°C 60%Rc is then acceptable.

**Table 3 :** Concrete creep model parameters

Basic Creep model parameters	
$\tau^{ref}$ (days)	15
$\epsilon_k^m$ (-)	3.4e-4
$\Delta P_{ref}^{CSH}$ (MPa)	0.35
$\tau_{ref}^{CSH}$ (days)	1

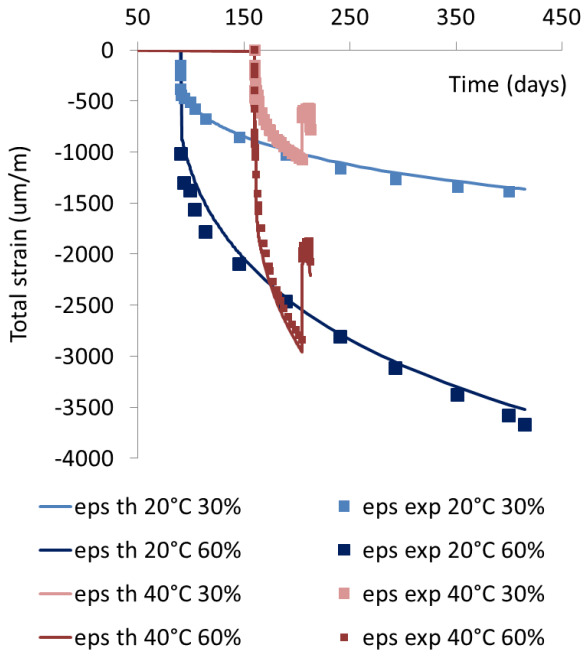


**Figure 6:** Concrete strain versus time since concreting. "th" for the simulation and "exp" for experimental results.

#### 4.2 Adjustment of data on a pre-stressed beam not loaded in flexion

The pre-stressed wire behavior law has been fitted on different tests carried on in the MACENA research project. The details of the model and its parameters for the wire are published in [5]. Figure 7 shows an application of the reinforcement behaviour law in the case of the relaxation test performed on a pre-stressed beam never loaded in flexion. The combination of the relaxation law for the wire and of the creep law for the concrete leads to a quite realistic stress variation in concrete only if the characteristic time  $\tau^{ref}$  is re-fitted with the strain results shown in figure 7, all the

other parameters fitted on cylinders are kept constant. The re-fitting of  $\tau^{ref}$  can be justified by the fact that, before pre-stressing, the concrete beams were stored a long time in the lab, and a parasite drying (not measured) had probably “pre-consolidated” the concrete by shrinkage, what can be considered in the model by an adjustment of the consolidation coefficient, which acts on the characteristic time in equations (7) and (11), this re-fitting method could be generalized to a real structure for which the concrete aging is unknown. Concerning the concrete stress shown in figure 7, it is measured indirectly by a setup allowing a continuous recording of the wire’s tension. This stress is then equal to the measured wire’s force divided by the cross section of the beam. This simulation constitutes also the beginning of the different cases of loading studied in the following section.

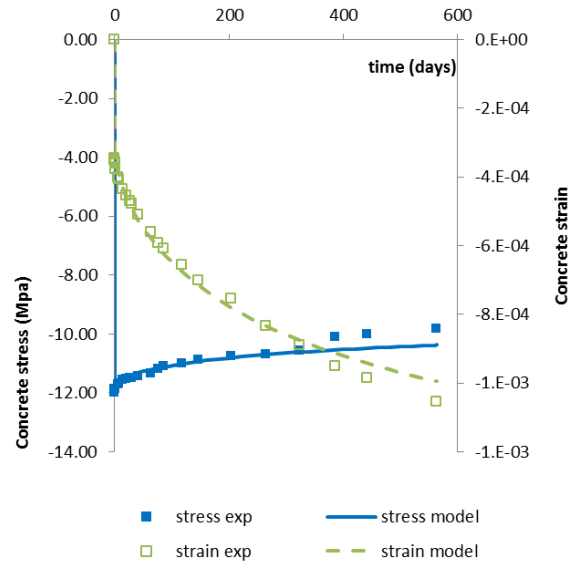


**Figure 7:** Simulation of the pre-stressed beam: evolution of concrete stress and strain versus time, comparison with experimental results after re-fitting of parameter  $\tau^{ref}$ .

### 5 SIMULATION OF THE PRE-STRESSED BEAMS IN BENDING AT DIFFERENT TEMPERATURES

Similar beams were tested at various dates. They were cast simultaneously, pre-stressed at

a same date but submitted to the bending loads and heated at different dates as specified in figure 9. The mesh used to compute these beams takes advantages of the two symmetry planes, allowing to only compute a quarter of each beam as illustrated in figure 8. The method of distributed reinforcements presented in section 3.1 (equation (1-2) and [7]) was used. The reinforcement’s densities ( $\rho_r$  in equation 1) are given in figure 8.

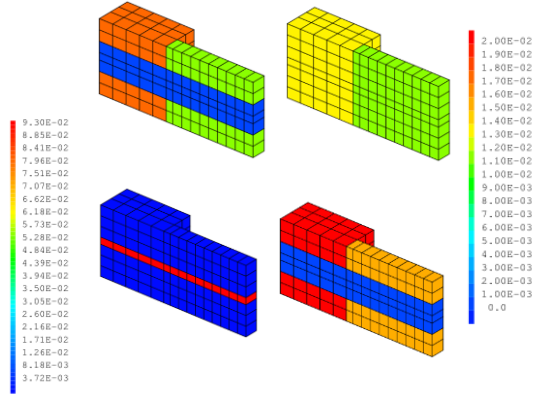


**Figure 8:** Mesh used to model the pre-stressed beams, volume fraction of reinforcement ( $\rho_r$  in eq. 1) per area. Density color scale for passive reinforcement on the right, for the wire on the left.

During the test, some experimental problems occur and have to be considered in the simulation. Particularly, a few days after bending (at 135 days for the beam at 40°C) et at 260 days for the beam at 20°C), the loading system turns from the imposed bending force to an imposed bending displacement, which needs to consider a change in a boundary condition of loading at these dates in the finite element simulations. Another problem was a parasite shift of the strain measured by the electric gauge located at the top of the mid span section for the beam stored at 40° C. So, the comparison between model predictions and experimental results in figure 9 consider all these particularities.

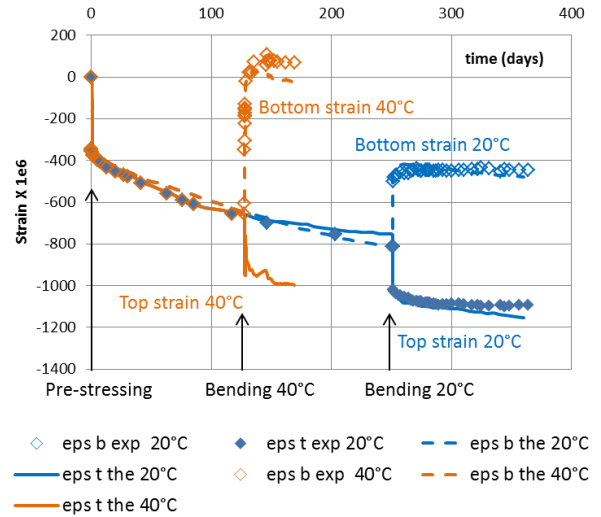


**Figure 9:** (the) Theoretical predictions of the strains at the top and bottom of the mid span section of the pre-stressed beams submitted to bending and heating at 20°C (blue) and 40°C (brown), and comparison with experiments strains (exp).

The results provided in figure 9, in terms of strains, allow verifying the aptitude of the model to capture the real behaviour of the beam. It is then possible, thanks to the internal variables of the model, to access to numerous results useful for engineers. Some of these fields are illustrated for the beam at 40°C in figure 10. In this figure, the stresses in concrete, wires and rebar can be easily analyzed.

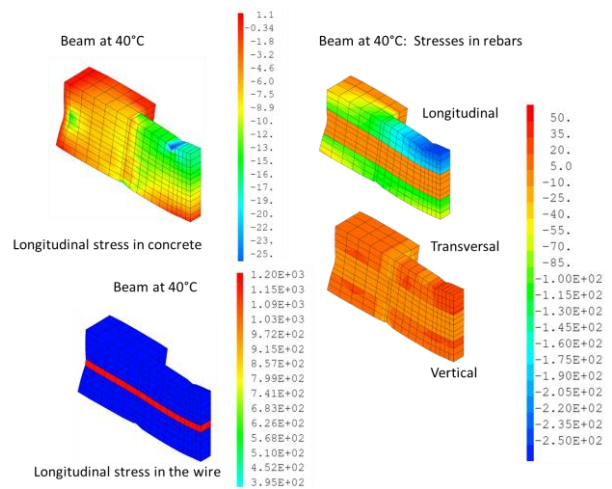


**Figure 10:** Stresses (MPa) predicted by the model at the end of bending period, in the different elements of the beam heated at 40°C.

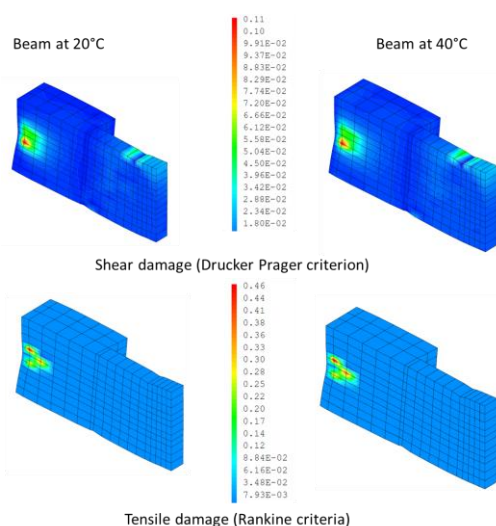


**Figure 11:** Damages predicted by the model at the end of bending period, in the different elements of the beam heated at 40°C.

The model provides also the damage level, as illustrated in figure 11. This figure shows that cracking occurs in the zone of introduction of pre-stressing. The bending load does not provoke tensile damages in the mid span section because the loss of pre-stressing before the bending is not sufficient to allow the tensile strength to be reached during the flexion stage, even at 40°C when the creep of creep and relaxation of the wire and are faster (figure 6), and the tensile strength reduced (figure 5).

## 12 CONCLUSIONS

Assessment of the stress states and of the damages induced by thermo-mechanical loading in reinforced pre-stressed concrete structures needs to merge several models and numerical methods. Each model needs experiments for fitting and validation. The French research project MACENA aspired at providing models and data for models usable to assess the behaviour of nuclear power plant vessels in case of loss of cooling accident. Among the different tasks envisioned in this project, the LMDC Toulouse aims to improve some aspects of numerical modeling, specifically the models concerning long term behaviour of concrete, wire and their interactions in a context of large structure

subjected to a thermo-mechanical loading. Several improvements were done in the domain of computational technics: homogenized reinforced concrete considering de-bonding of reinforcements [7], concrete creep modeling [4], wire relaxation [5], dependence of concrete parameters to temperature [14–16]. Once merged, these models are tested on laboratory experiments including concrete cylinders and pre-stressed beams in different conditions of loading and temperature. The paper summarized the main originalities of the resulting model and its ability to simulate a thermo-mechanical loading of a prestressed structure. Other tests and developments are required before applying it to a real nuclear power plant vessel. Among them, the consideration of higher temperatures, and other moistures conditions have to be validated.

## AKNOWLEDGEMENTS

The French National Research Agency (ANR) is thanked for its financial support to the research projects MACENA and MOSAIC, the French national agency for atomic and alternative energy (CEA) is also thanked for providing the finite element code Castem.

## REFERENCES

- [1] Cagnon H, Vidal T, Sellier A and Torrenti J M 2016 Transient Thermal Creep at Moderate Temperature *Key Eng. Mater.* **711** 885–91
- [2] Nguyen V N, Cagnon H, Vidal T, Torrenti J . and Sellier A 2017 Effet des couplages Thermo-Hydro-Mécaniques sur le comportement différé du béton précontraint *23ème Congrès Français de Mécanique, Lille, 28 Août au 1er Septembre* (Lille (France)) p 16
- [3] Sellier A, Casaux-Ginestet G, Buffo-Lacarrière L and Bourbon X 2012 Orthotropic damage coupled with localized crack reclosure processing Part II: Applications *Eng. Fract. Mech.* **97**
- [4] Sellier A, Multon S, Buffo-lacarrière L,

- Vidal T, Bourbon X and Camps G 2016 Concrete creep modelling for structural applications: non-linearity , multi-axiality , hydration , temperature and drying effects *Cem. Concr. Res.* **79** 301–15
- [5] Chhun P, Sellier A, LacARRIERE L, Chataigner S and Gaillet L 2018 Incremental modeling of relaxation of prestressing wires under variable loading and temperature *Constr. Build. Mater.* **163** 337–42
- [6] Toumi Ajimi W, Chataigner S, Falaise Y and Gaillet L 2016 Experimental investigations on the influence of temperature on the behavior of steel reinforcement ( strands and rebars ) *CONSEC 2016* ed I C on C in S Conditions p 8
- [7] Sellier A and Millard A 2019 A homogenized formulation to account for sliding of non-meshed reinforcements during the cracking of brittle matrix composites: Application to reinforced concrete *Eng. Fract. Mech.* **213** 182–96
- [8] Chhun P 2017 *Modélisation du comportement thermo- hydro -chemo-mécanique de s enceinte s de confinement nucléaire en béton armé - précontraint* (Université de Toulouse, INSA, UPS)
- [9] Bucher R, Sellier A, Verdier J and Vidal T 2017 *Effet de la microfissuration de séchage sur les propriétés mécaniques et de transfert des matériaux cimentaires* (Toulouse)
- [10] Bouhjiti D E-M, Boucher M, Briffaut M, Dufour F, Baroth J and Masson B 2018 Accounting for realistic Thermo-Hydro-Mechanical boundary conditions whilst modeling the ageing of concrete in nuclear containment buildings: Model validation and sensitivity analysis *Eng. Struct.* **166** 314–38
- [11] Ladaoui W, Vidal T, Sellier A and Bourbon X 2011 Effect of a temperature change from 20 to 50C on the basic creep of HPC and HPFRC *Mater. Struct.* **44** 1629–39
- [12] Ladaoui W, Vidal T, Sellier A and Bourbon X 2013 Analysis of interactions between damage and basic creep of HPC and HPFRC heated between 20 and 80 °C *Mater. Struct.* **46** 13–23
- [13] Manzoni F, Vidal T, Sellier A and Bourbon X 2019 Modeling of Transient Thermal Deformation in temperature and application to disposal tunnels for medium activity exothermic nuclear wastes 1 *9th international conference on concrete under severes conditions-environnement & loading* (Porto Alegre) pp 1–10
- [14] Kallel H, Carré H, Laborderie C, Masson B and Tran N C 2016 influence of Moisture and Temperature on Mechanical Properties of the Concrete *Framcos '9* (Berkeley, California, USA: IA-FraMCoS)
- [15] Buffo-LacARRIERE L, Sellier A, Kolani B, Souyris P and Chhun P 2015 Early age behaviour of reinforced concrete. Lessons from numerical case studies *SSCS conference* ed R et. Al. (14-16 dec, Rio de Janeiro.)
- [16] Chhun P, Buffo-LacARRIERE L and Sellier A 2016 Material and Geometric Heterogeneity Consideration for Cracking Risk Prediction of Young Age Behavior of Experimental Massive Reinforced Concrete Structure *Key Eng. Mater.* **711** 900–7